

# An Investigation Into Key Influence Factors for the Everyday Usability of Electric Vehicles

ADAM THOR THORGEIRSSON <sup>1,3</sup>, STEFAN SCHEUBNER<sup>2,3</sup>, SEBASTIAN FÜNFELD<sup>1,3</sup>,  
 AND FRANK GAUTERIN <sup>3</sup>

<sup>1</sup>Dr. Ing. h. c. F. Porsche AG, Department of Energy Management, R&D Center Weissach, Germany

<sup>2</sup>Department of E-Mobility Charging Infrastructure, EnBW AG, 76131 Karlsruhe, Germany

<sup>3</sup>Institute of Vehicle System Technology, Karlsruhe Institute of Technology, 76131 Karlsruhe, Germany

CORRESPONDING AUTHOR: ADAM THOR THORGEIRSSON (e-mail: adam\_thor.thorgeirsson1@porsche.de)

This work was supported by the KIT-Publication Fund of the Karlsruhe Institute of Technology.

**ABSTRACT** Society relies on electric mobility to decrease the problems associated with local emissions and global climate change. One key factor for the success of electric vehicles is their everyday usability. Today's users must deal with limited driving range in a sparse charging infrastructure. In this work, we investigate central features influencing the everyday usability of electric vehicles, such as battery capacity, charging infrastructure, range prediction accuracy and vehicle concepts. Since the influence of these aspects depend on each other, they cannot be examined separately. Therefore, we created a stochastic simulation framework with vehicle models and map data to calculate a large amount of different feature variations. One of our key findings is that battery capacities beyond 100 kWh are not feasible. In addition, we stated the importance of an accurate range estimation algorithm and a dense network of high-performance charging points for everyday usability. Taking these results into consideration would help policy makers and automobile manufacturers achieve worldwide acceptance of electric vehicles.

**INDEX TERMS** Range estimation, electric vehicles, charging infrastructure, stochastic simulation.

## I. INTRODUCTION

In recent years, electric mobility has become more important and present. Car manufacturers are launching more battery electric vehicles (BEVs) and charging infrastructure is being expanded both by government agencies as well as private establishments. Policy makers want to increase the numbers of BEVs by introducing subsidies or even by banning internal combustion engine powered vehicles (ICEVs) from urban areas. However, due to the limited charging infrastructure and the lower driving range of BEVs, drivers experience range anxiety, which is the fear of stranding with an empty battery.

To achieve widespread acceptance of electric mobility, range anxiety must be eliminated and the everyday usability of the vehicles increased. Thus, an appropriate charging infrastructure has to be available. A dense network of high-performance charging points has to be installed such that a user neither has to worry where a charging point is, nor has to wait a long time while charging. In addition, the battery capacity must be high enough to ensure sufficient driving

range. Thereby, technical, economical and environmental restrictions impact the dimensioning of the battery. Following that, battery capacities must be *large enough* for public acceptance while minimizing negative technical, economical and environmental effects. Lastly, the range estimation algorithm within the vehicle must be reliable enough so the driver does not end up being stranded with an empty battery, due to an over-optimistic prediction.

We want to investigate *how many* and *where* the charging points (CPs) should be, *how accurate* a range estimation algorithm has to be and *how big* batteries need to be to ensure everyday usability of BEVs. Previous work on this topic has been done with limited granularity.

When looking at the everyday usability, the usual approach is to compare the total ranges of BEVs with trip statistics from mobility surveys or driving profiles collected with GPS trackers [1], [2]. A significant drawback of this approach is the variability in energy consumption and range between different scenarios which is not included. Moreover, [3] found that

mobility surveys alone are not enough to evaluate feasibility and the everyday usability. A review of different studies using driving profiles was recently given by [4].

In the majority of published results, charging stops are either neglected or severely simplified with assumptions about the availability of CPs [5]–[8]. Researchers rather tend to assume that no charging should be necessary to make BEVs feasible [9]–[14]. Driving profiles as well as simulations have been used to determine optimal CP positioning [15]–[17], CP power demand [18]–[23] as well as for battery lifetime analysis [24].

In our paper, we introduce a detailed simulation framework to analyze the everyday usability of battery electric vehicles (BEVs). The framework includes current road and charging infrastructure, in which a realistic range estimation, charge planning as well as vehicle simulation is carried out. The simulated vehicles are based on a powertrain model and can be adapted to different vehicle concepts. One simulation in the framework consists of a single trip which comprises driving and possible charging stops. Thereby, we can calculate a multitude of realistic scenarios by random trip generation, where total trip duration is our measure for the everyday usability. The results provide indications for required advances in charging infrastructure and battery capacity to optimize the total trip duration.

This paper is organized as follows: Section II introduces our overall methodology including the powertrain model used to simulate energy consumption. Then, Section III shows the range estimation model, which is the basis for our charge planning algorithm. Section IV presents the actual trip simulation framework and the analysis of the key factors concerning everyday usability of BEVs. The results of the simulations are shown subsequently in Section V before the paper is concluded in Section VI.

## II. METHODOLOGY

### A. NOTATION

According to typical mathematical convention, bold letters represent vectors, e.g.  $\mathbf{x}$ , whereas  $x$  denotes a scalar. A tilde on top of a value denotes a forecasted value  $\tilde{x}$  and a bar denotes an average  $\bar{x}$ . If a variable is the result of an estimation process, it is signified with a hat  $\hat{x}$ . The expression  $\Pr(x)$  stands for the probability of  $x$ .

### B. OVERVIEW

The overall approach of our work is schematically presented in Fig. 1. Fundamentally, it consists of a simulation framework, which first chooses a vehicle type with specific battery properties. Then, a random trip is drawn and the charge planning is executed to find required charging stops on the trip. Subsequently, the simulated vehicle drives the virtual trip and results are generated, which, in turn, can be thoroughly analyzed.

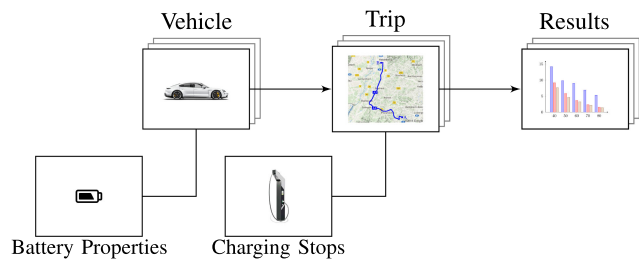


FIGURE 1. Overall approach of the simulation framework.

The factors investigated by the simulation are vehicle type, battery properties, charging infrastructure and range prediction accuracy. Among these factors, the range prediction accuracy receives comparatively less attention in related research. However, this factor is of high importance, as charge planning relies on the range estimation. Consequently, high errors in range prediction accuracy could have a considerable effect on the everyday usability of BEVs. Therefore, we want to emphasize range estimation accuracy as one of the key factors in Section III.

### C. ENERGY CONSUMPTION MODEL

An energy consumption model is necessary for both the range estimation algorithm shown in Section III and for the trip simulation in Section IV. This section introduces the model used in this work. This model has previously been used in the related works: [25]–[27].

To calculate tractive energy consumption  $E_c$ , first, the driving resistances  $F_r$  must be calculated according to the standard driving resistance model [28]. The following equation explains this model, with vehicle mass  $m$ , gravitational acceleration  $g$ , rolling resistance coefficient  $f_r$ , aerodynamic drag coefficient  $c_w$ , air density  $\rho$ , vehicle frontal area  $A$ , road gradient angle  $\alpha$ , vehicle velocity  $v$  and acceleration  $a$ .

$$F_r = \underbrace{\begin{pmatrix} m f_r \\ 1/2 c_w \rho A \\ m \end{pmatrix}}_{\mathbf{p}} \cdot \underbrace{\begin{pmatrix} g \cos \alpha \\ v^2 \\ a + g \sin \alpha \end{pmatrix}}_{\mathbf{B}} \quad (1)$$

Note that the vehicle parameter vector  $\mathbf{p} \in \mathbb{R}^{3 \times 1}$  concentrates the individual vehicle properties. These can be adjusted to the specific test vehicle at hand with help of test bench measurements. Also, they can be estimated e.g. with help of a Kalman filter, as shown in [25].

After calculating the driving resistances  $F_r$  of the vehicle, the powertrain efficiency has to be determined. The powertrain losses  $\eta_{PT}$  can be included using characteristic maps of the powertrain components. These comprise wheels, gearbox (GB), electric motor (EM) and power electronics (PE), as shown in Fig. 2. The model requires  $F_r$  and vehicle speed  $v$  as inputs to obtain energy consumption  $E_c$ , thus the degree of

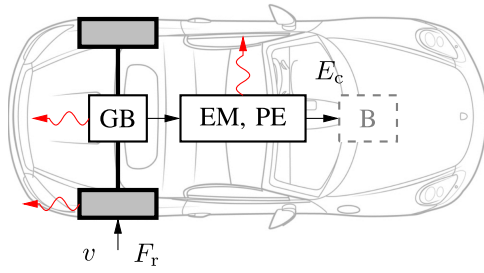


**FIGURE 2.** Powertrain model with input variables  $F_r$ ,  $v$  and output variable  $E_c$ . The red arrows indicate simulated component losses.

efficiency is also dependent on these values:

$$\eta_{PT} = f(F_r, v). \quad (2)$$

In the case of negative  $F_r$ , the regenerated energy is calculated based on the combined efficiency map of the electric motors and power electronics at nominal battery voltage, without consideration of other influences, e.g. additional mechanical braking for high deceleration phases. We use vehicle parameters from test bench measurements with an electric PORSCHE BOXSTER. This model was already validated using real test drives in [27] and is applied without changes.

### III. RANGE ESTIMATION

The apparent task of range estimation is the indication of the *distance-to-empty* to the driver. This is known even from internal combustion engine powered vehicles (ICEVs). In addition, when planning a long distance trip with an electric vehicle, range estimation helps to calculate the optimal charging stop by predicting the energy demand on a chosen route  $\tilde{E}_c$ . Comparing  $\tilde{E}_c$  with the battery's energy  $\hat{E}_b$  results in the attainability of a specific destination. Among the attainable charging stops, the navigation software is able to choose the best option, e.g. the CP with highest charging power. However, most drivers feel that their range estimation is not reliable and reserve a part of the capacity as safety margin  $\Delta b_E$ , e.g. 20% in [29]. Therefore, a destination such as a CP is deemed attainable if

$$\tilde{E}_c \leq (1 - \Delta b_E) \hat{E}_b. \quad (3)$$

Thus, with a more accurate and reliable range estimation algorithm, drivers will use more of the installed capacity and therefore, more of their range between charging stops. Higher utilization of capacity translates into higher everyday usability of the vehicle, a key issue for electric vehicles. In the following section, we introduce the process of obtaining  $\tilde{E}_c$ . The value for  $\hat{E}_b$  is obtained from the vehicle's measurement system.

#### A. DATA ACQUISITION

Some of the algorithms used for range estimation learn from driving data to generate forecasts, e.g. of the future driving speed  $\tilde{v}$ . The driving data used here comes from real test drives in various locations and with various drivers. However, they

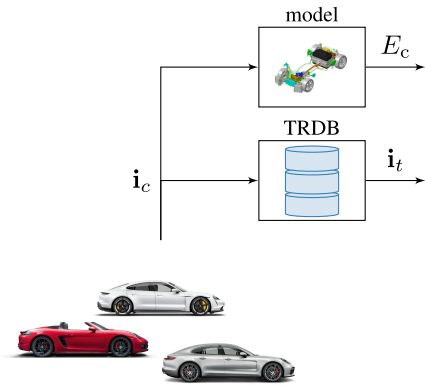


**FIGURE 3.** Data acquisition method.

**TABLE 1.** Details About the Datasets

	anonymous	driver-specific
total distance	3081 km	1896 km
mean speed	$23.7 \text{ m s}^{-1}$	$28.4 \text{ m s}^{-1}$
highway percentage	68 %	87 %
number of map segments $k$	14621	8800
number of drivers	unknown	10
number of trips	68	20

also have been executed with a multitude of different vehicles and configurations (e.g. powertrain topology, number of passengers). Therefore, the energy consumption differs within the test set. To make it comparable, we used the original driving data  $\mathbf{i}_c$  as an input for a validated simulation model, which subsequently outputs the equivalent energy consumption  $E_c$ . The simulation model has a specific vehicle configuration, and thus, the energy consumption values are comparable. In addition, the test set is enriched with information from a traffic and routing database (TRDB)  $\mathbf{i}_t$ . Such databases are known to users from GOOGLE MAPS or HERE MAPS. In these databases, a route comprises several segments  $k$  with a list of properties such as gradient  $\alpha_k$ , street class  $\Lambda_k$ , mean traffic speed  $\bar{u}_k$ , road curvature  $\kappa_k$ , legal speed limit  $v_{lim,k}$ , segment length  $l_k$  etc. In this work, the traffic and routing database (TRDB) of HERE is used, see [30] for a documentation. For each test drive, traffic speed is obtained from the TRDB matching the exact time and date of departure of the real test-drive. An illustration of the data acquisition approach can be seen in Fig. 3.

We use two different datasets in this work. One is called *anonymous* and comprises test drive data of unknown drivers in Germany, France, Austria and Belgium. The other dataset is called *driver-specific*, where the drivers are known. This allows the algorithms to be trained for individual drivers, yielding personalized parameters. The driver-specific data was collected in Germany. More details can be found in Table 1. The data was collected with the goal of covering different drivers, road infrastructure as well as traffic situations, but the statistical representativeness of the dataset can never be fully verified.

### B. TRACTIVE ENERGY DEMAND PREDICTION

The central part of range estimation is the energy demand prediction (EDP) which is presented in this section. In this section, we focus on the tractive energy, which is the amount of energy needed for the vehicle’s forward motion and does not include auxiliary equipment (HVAC, infotainment etc.). Tractive energy is the biggest part of the total energy consumption and depends on physical influences e.g. elevation profile and rolling resistance as well as non-deterministic influences e.g. traffic and driver behavior.

To obtain a prediction of the tractive energy demand on a given route, (1) can be used. Assuming the vehicle properties will not change, only a forecast of the driving data  $\tilde{\mathbf{B}}$  is required. The necessary information about gradient and vehicle speed on the selected route is part of the traffic and routing database (TRDB).

Looking at  $\tilde{\mathbf{B}}$ , the values for  $\tilde{\alpha}$ ,  $\tilde{v}$  and  $\tilde{a}$  must be obtained. Technically, the gradient angle  $\tilde{\alpha}$  is not a predicted value, as it is a geometrical constant that can be obtained from the map. In contrast, the forecast for  $\tilde{v}$  and  $\tilde{a}$  translates to future driving behavior on the given route and is, therefore, difficult to predict. A common approach is to use the mean traffic speed  $\bar{u}_k$  as an approximation for  $\tilde{v}$ . This approach assumes future driving behavior of a specific vehicle is similar to the driving behavior of all vehicles on the road. The future acceleration  $\tilde{a}$  is not included in the TRDB data, which only contains speed values. A possible approach would be to assume constant acceleration between map segments  $k$  and then calculate  $\tilde{a}$  from the speed difference between  $\bar{u}_k$  and  $\bar{u}_{k+1}$ . However, in this work we use the method of [27] and calculate the change in kinetic energy  $\Delta E_{kin}$  between the segments. As a result, the predicted energy on a segment  $\tilde{E}_{c,k}$  is the sum of the energy prediction, not including acceleration  $\tilde{E}_{c|a=0}$  and the kinetic energy change  $\tilde{E}_{c,k}$ :

$$\tilde{E}_{c,k} = \underbrace{\int \frac{\tilde{F}_{r,k}}{\eta_{stat}(\tilde{F}_{r,k}, \tilde{v}_k)} ds}_{\tilde{E}_{c|a=0}} + \underbrace{\frac{m}{2\eta_{dyn}} [(\tilde{v}_{k+1})^2 - (\tilde{v}_k)^2]}_{\Delta E_{kin}}. \quad (4)$$

A dynamic degree of efficiency  $\eta_{dyn}$  is introduced, as otherwise, the model would assume that a kinetic energy change is free of losses. However, since the powertrain losses are already included in  $\eta_{stat}$ , this paper assumes a mild loss factor of approximately 0.9 for  $\eta_{dyn}$ .

In summary, the only value that needs to be predicted is the velocity  $\tilde{v}$ . The algorithms for velocity prediction (VP) are introduced in Section III-C. After that, the model is able to calculate  $\tilde{E}_c$ . The complete approach is illustrated in Algorithm 1.

### C. VELOCITY PREDICTION

While the assumption of  $\tilde{v} = \bar{u}$  is common in modern systems, research suggests using data-based learning models to predict future driving speed. There are many different candidate algorithms of different complexity. In this work, a selection of algorithms is investigated and their results are compared

---

#### Algorithm 1: Range Prediction.

---

```

simulate  $E_c$  for available test drive data
download  $\mathbf{i}_t$  for test drives
for  $n < total\ test\ drive\ count$  do
    split driving data into training and test
    train velocity prediction (MLR, SVM)
    predict  $\tilde{E}_c$  for test data
    evaluate weighted absolute error (WAE)

```

**Result:** WAE for MLR, SVM,  $\bar{u}$

---

against the initial assumption of future driving speed being equal to mean traffic speed.

#### 1) LINEAR REGRESSION

A simple model among candidate algorithms is the linear regression. It assumes a linear relationship between features and output variable  $\tilde{v}$ . Using this linear model for multi-dimensional inputs requires multi-linear regression (MLR), which is the straight-forward extension of the scalar model to a vector model [31], [32]. The connection, or *pattern*, describing the dependency of  $\tilde{v}$  on the features is expressed with the hypothesis vector  $\mathbf{h}$ . After the pattern has been identified using training data, the forecast can be made with help of the predicted features for the selected route. Finding the hypothesis vector gives the following minimization problem:

$$\min_{\mathbf{h}} \sum_{k=1}^n \Theta \left( \tilde{v}_k - \mathbf{h} \cdot [\bar{u}_k \ v_{lim,k} \ \kappa_k \ \Lambda_k \ \bar{\alpha}_k]^T \right). \quad (5)$$

Obtaining optimal  $\mathbf{h}$ , which results in the smallest overall deviation from the measured speed  $\tilde{v}$  on all segments  $n$  of the training data, is dependent on the loss function  $\Theta$ . The standard least-squares (LS) loss function would have the weight function  $\Theta = (\cdot)^2$ . However, least-squares (LS) is not robust, therefore in the multi-linear regression (MLR) implementation in this work, the Huber loss function is used for  $\Theta$  to limit outlier weights [33]. In addition, the observations are linearly weighted according to segment length  $l_k$ , hence longer segments are more important for the regression than shorter segments. To generate a forecast, the hypothesis  $\mathbf{h}$  from the training data and the features from the future trip are required. Thereby the forecast  $\tilde{v}$  is the result of the direct computation  $\mathbf{h} [\cdot]^T$ .

#### 2) SUPPORT VECTOR REGRESSION

Previously, a linear model was used for velocity prediction (VP). Since driving behavior comes down to human behavior, the system could also be non-linear, which could lead to inadequate representation by the multi-linear regression (MLR). Therefore, a more complex model should be implemented for comparison. Among candidate algorithms for pattern analysis, support vector regression (SVM) has been demonstrated as a suitable candidate for travel time prediction by [34], which is a similar application. In a traffic speed forecast project [35], the

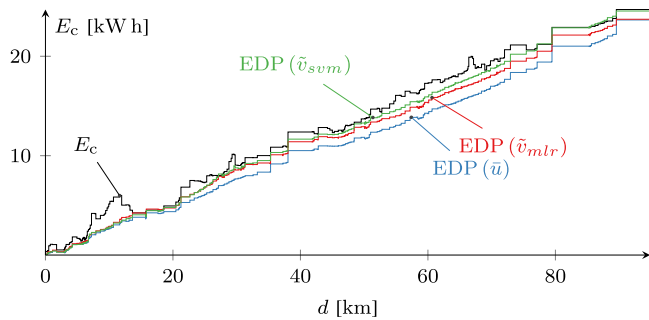


**FIGURE 4.** EDP example from the anonymous dataset.

performance of an support vector regression (SVM) was compared to a neural network, which is one of the most common machine learning algorithms nowadays. It was shown that SVM produced more accurate results, especially when dealing with limited training data quality and quantity. Based on these assessments, where the features were limited to probe data, we choose SVM as the candidate machine learning algorithm for the velocity prediction (VP) algorithm implemented in this work. The SVM implementation of [36] was used with a polynomial kernel with the same features as the MLR, therefore the reader is referred to the literature for more details about the algorithm itself.

#### D. PERFORMANCE EVALUATION

With help of the velocity prediction (VP) introduced in the previous section, the energy demand prediction (EDP) can be calculated. In consequence, there are three possibilities: (1) energy demand prediction (EDP) with mean traffic speed  $\bar{u}$ , (2) EDP with  $\tilde{v}$  from SVM and (3) EDP with  $\tilde{v}$  from MLR. Theoretically, the performance of the algorithms should follow their order of complexity. However, even if this would be the case, the question remains whether the performance improvement is worth the increased complexity. As the prediction error must be obtained, consideration of its calculation also falls within the scope of this paper. An exemplary prediction with all three approaches using the anonymous dataset is illustrated in Fig. 4. The correct energy consumption along the trip is depicted in black, originating from the real test drive data.

In this example, SVM shows the best performance. To investigate whether this is true for all the test data, the following performance evaluation is executed using *cross-validation*. For the anonymous dataset, five trips are used as learning data and one trip as test data. For the driver-specific dataset, there are always two trips per driver. One trip is used for training, the other for testing and vice versa. The error measure used to express the overall prediction error is the weighted absolute error (WAE):

$$WAE = \frac{\sum_i |\tilde{E}_{c,i} - E_{c,i}| \cdot l_i}{\sum_i l_i} \quad (6)$$

**TABLE 2.** Performance of the EDP on the Anonymous Dataset

	WAE	$\mu$	$\sigma$
$EDP_k(\tilde{v}_{svm})$	1.246 kWh	$-0.012 \text{ W h m}^{-1}$	$0.028 \text{ W h m}^{-1}$
$EDP_k(\tilde{v}_{mlr})$	1.230 kWh	$-0.008 \text{ W h m}^{-1}$	$0.022 \text{ W h m}^{-1}$
$EDP_k(\bar{u})$	1.085 kWh	$-0.007 \text{ W h m}^{-1}$	$0.021 \text{ W h m}^{-1}$

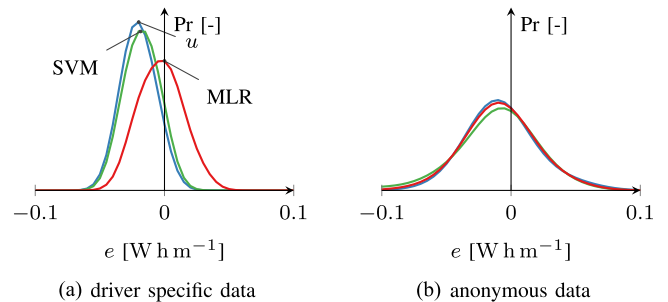


**FIGURE 5.** Error of the energy demand prediction (EDP). Fig. 5 a illustrates the result on the driver-specific dataset and Fig. 5 a shows the result for the anonymous dataset.

The WAE results for EDP as well as mean value  $\mu$  and standard deviation  $\sigma$  are shown in Table 2 for the anonymous dataset. Upon first glance, the result is surprising: the order of WAE results is inverse compared to the algorithm complexity. The best result comes from simply using mean traffic speed  $\bar{u}$  followed by the linear regression  $\tilde{v}_{mlr}$  and the worst result is obtained by the support vector regression  $\tilde{v}_{svm}$ . The same order holds for mean value and standard deviation.

However, when looking at the same error measures for the algorithms on the driver-specific dataset, the resulting order fits better to the expectation. The worst WAE result is obtained when no forecast algorithm is used and future velocity equals mean traffic speed  $\bar{u}$ . Still, MLR is superior to the more complex algorithm of SVM. This means that an increase in prediction accuracy is gained by learning driving behavior, however even a simple algorithm, such as MLR, is sufficient to realize this advantage.

Fig. 5 illustrates the overall error on all trips with help of Kernel density estimations in terms of  $\text{Whm}^{-1}$ . It can be seen once again that for driver-specific data, MLR is the best option. For anonymous data, the algorithms show similar performance, and thus a complex algorithm is not worth implementing. In the following section, the resulting range estimation accuracy is examined on whether it influences the everyday usability of electric vehicles.

#### IV. DRIVE SIMULATION FRAMEWORK WITH CHARGING INFRASTRUCTURE

In this section, the investigation of the interaction between range estimation, vehicle properties, road network and charging infrastructure is presented. To investigate this, a simulation framework is developed, where these parameters can be varied. The basis of the simulation model is a road network with charging infrastructure and a BEV powertrain model. The individual steps performed are shown in Algorithm 2.

TABLE 3. Performance of the EDP on the Driver-Specific Dataset

	WAE	$\mu$	$\sigma$
$EDP_k(\tilde{v}_{svm})$	1.655 kW h	-0.018 W h m <sup>-1</sup>	0.011 W h m <sup>-1</sup>
$EDP_k(\tilde{v}_{mlr})$	1.163 kW h	-0.003 W h m <sup>-1</sup>	0.015 W h m <sup>-1</sup>
$EDP_k(\tilde{u})$	1.883 kW h	-0.02 W h m <sup>-1</sup>	0.01 W h m <sup>-1</sup>

**Algorithm 2:** Simulation Process.

```

choose vehicle
draw start SoC
draw route start and destination points
get fastest route  $\pi$ 
predict energy consumption  $\tilde{E}_c$ 
if  $\tilde{E}_c > (1 - \Delta b_E) \hat{E}_b$  then
  | plan charging stops
simulate trip with BEV powertrain model
Result: trip data
  
```

First, a vehicle is chosen with specific vehicle properties such as mass  $m$ . Then, the state of charge (SoC) at the beginning of the trip is selected, which defines the battery energy content  $\hat{E}_b$ . The SoC at the beginning of a trip is drawn from a uniform distribution ranging from 40% to 100%. Thereby, distinct charging opportunities at the start locations are represented. Subsequently, the desired length of the trip is set, random start and endpoints on the map are selected and the fastest route between them is calculated. Predicting  $\tilde{E}_c$  with the EDP model presented in the previous section, indicates whether charging is required during the trip. If necessary, charging stops are added to the trip. Lastly, the trip is simulated, generating virtual test drive data. To obtain insights into key influences for trip duration, we simulate hundreds of thousands of trips with different vehicles, vehicle parameters and charging infrastructure combinations. In the remainder of this section, the individual steps in the simulation framework are explained in detail.

**A. VEHICLES AND THEIR PROPERTIES**

To increase the level of detail of the analysis, the framework includes three types of general, synthetic vehicles:

- small vehicle
- mid-size vehicle
- large vehicle / SUV

The vehicles are all based on the topology shown in Fig. 2, but have different characteristic parameters, leading to different energy consumption behavior. These parameters are vehicle mass  $m$ , aerodynamic drag area  $c_dA$ , tire rolling resistance  $f_r$  and a loss factor  $C_L$ . The loss factor describes the component losses in relation to a mid-size vehicle’s powertrain, which serves as a benchmark. An overview of these parameters and the corresponding mean consumption is given in Table 4.

For each vehicle, the battery capacity is variable. This means that the total vehicle mass  $m$  is also variable and is a

TABLE 4. Vehicle Data

	small	mid-size	large
$c_dA$ [m <sup>2</sup> ]	0.48	0.62	0.84
$m$ [kg]	1435	2200	2600
$f_r$ [-]	0.0062	0.0090	0.0090
$C_L$ [-]	0.8	1	1.1
$dE_c/ds$ [W h m <sup>-1</sup> ]	0.166	0.214	0.254

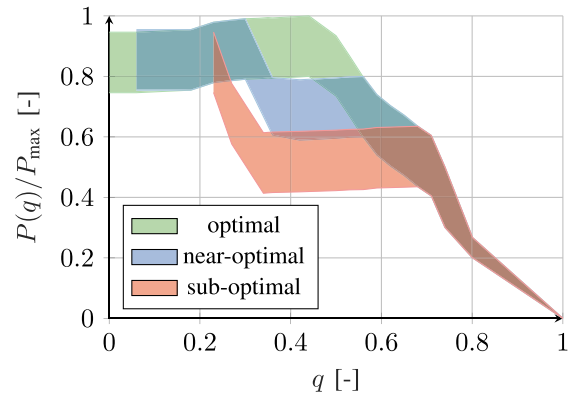


FIGURE 6. Characteristic battery charging power curves as a function of battery state of charge  $q$ , for three different levels of pre-conditioning.

function of battery capacity:

$$m = m_V + m_B(Q), \tag{7}$$

where  $m_B$  is the battery mass as a function of capacity  $Q$  and  $m_V$  is the mass of the rest of the vehicle.

Another important battery specification is the charging power, which is dependent on various factors such as charging strategy and thermal conditions [37]. Modern BEVs are equipped with systems that pre-condition the battery before charging, to maximize the possible charging power at a charging stop [38]. Dependent on driving profile and ambient temperature, optimal conditions may not be reached at all times. Furthermore, the SoC at the beginning of the charging session is important. Based on data published by TESLA drivers [39] and our experiences with PORSCHE BOXSTER and PORSCHE TAYCAN BEVs, we define three characteristic charging power curves for different levels of pre-conditioning and initial SoC. Fig. 6 shows the characteristic curves for the charging power dependent on SoC  $q$ . Each of the charging curves includes an uncertainty margin, to account for variability in driving profile, environment conditions and CP performance. The three levels of pre-conditioning are optimal, near-optimal and sub-optimal. The optimal charging curve can be assumed if the initial SoC is low and battery temperature is within optimal range. In case of higher initial SoC or battery temperatures below the optimal range, near-optimal or sub-optimal pre-conditioning levels can be assumed. In the simulation framework, a random variable following a multinomial distribution indicates the level of pre-conditioning attained at a given charging stop. For a higher SoC at the beginning of the charging,

the probability of a less-optimal charging curve is higher. Nevertheless, if a CP's available charging power is lower than the characteristic charging curve, then the CP is the limiting factor. The most powerful public high-performance CPs can deliver a charging power of up to 350kW [40]. Nonetheless, the vast majority of CPs can only charge with 50kW or less [41].

The maximum charging power is dependent on the electrical current flowing in each battery module. A battery's peak *C-Rate* is defined as the ratio:

$$C\text{-Rate} = \frac{P_{max}}{Q}, \quad (8)$$

where  $P_{max}$  is peak charging power and  $Q$  is battery capacity. The PORSCHE TAYCAN has a peak *C-Rate* of about  $270\text{kW}/93.4\text{kWh} = 2.89\text{h}^{-1}$  [40] and the TESLA MODEL 3  $250\text{kW}/75\text{kWh} = 3.33\text{h}^{-1}$  [38].

When battery modules are removed from a battery pack to reduce total capacity, the maximum charging power is reduced to keep a constant *C-Rate*. However, if package space is not a limitation,  $P_{max}$  could theoretically be kept constant with reduced capacity, by re-designing the battery pack with a new nominal capacity [42]. To scale the characteristic charging curves for different capacities, i.e. for a different number of battery modules, the following relation can be used:

$$P(q, Q) = P^{(nom)}(q) \frac{C\text{-Rate}_{max}}{P_{max}^{(nom)}/Q}, \quad (9)$$

where  $P^{(nom)}(q)$  is the charging power at SoC  $q$  and  $P_{max}^{(nom)}$  is the maximum charging speed of the battery pack at nominal capacity. In this work, we choose a maximum *C-Rate* of  $3\text{h}^{-1}$ , and  $P_{max}$  of 270kW.

## B. TRIP SAMPLING

To achieve an accurate analysis of BEV driving, the trips should be chosen so that they resemble typical mobility patterns and driver behavior. The trips in this work are restricted to the region in which our test-drives were carried out. We define the region by parallels  $47^\circ\text{N}$  and  $54.5^\circ\text{N}$  and meridians  $4^\circ\text{E}$  and  $14^\circ\text{E}$ , as shown in Fig. 8. The region includes parts of Germany, the Netherlands, Belgium, Luxembourg, France, Switzerland, Liechtenstein, Austria and the Czech Republic and shows diversity in road and charging infrastructure as well as in population density.

To generate realistic mobility patterns, empirical probability distributions are used to draw samples for

- route length
- time of departure
- start and destination positions

In real life, a driver's daily mileage is usually shorter than 72km [43]. According to the *US National Household Travel Survey*, only 9.8% of trips are 21 miles (33.8km) or longer [44]. A European survey (France, Germany, Italy) showed that an average personal trip distance is approximately 16km and an average business trip approximately 20km. The average

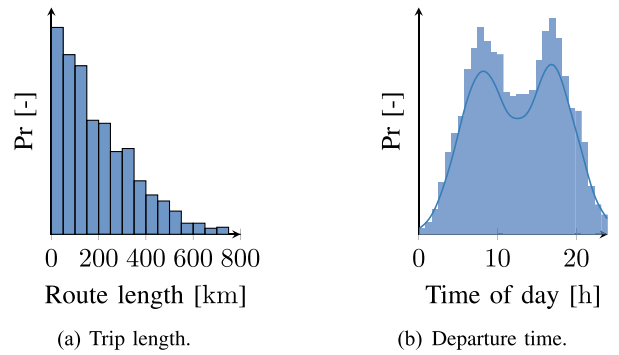


**FIGURE 7.** Trip length and departure time distributions for the trip sampling.

daily driven distance is approximately 55km and approximately 70% of daily driving does not exceed 50km [45].

In this work, the main goal is to analyze the everyday usability of BEVs. A primary concern regarding BEV usability is their suitability for longer trips. Therefore, we choose a total distribution of trip distances with a significant bias toward long-distance trips longer than 100km, when compared to mobility surveys. Fig. 7 a shows a histogram of the distances of the sampled routes. The median distance is 154km. The time of departure is relevant for the traffic state in the trip data. The traffic state influences the driving speed which has a direct influence on the vehicle's energy consumption. For departure time, we chose a uniform distribution for the day of the week and a two modal normal distribution for the time of day, with modes at 8:00 in the morning and 17:00 in the afternoon as shown in Fig. 7 b.

For each trip, the start and destination point samples are drawn from population data that include estimates of population count for 30 arc-second grid cells [46]. Fig. 8 shows a countour plot of the population data in the chosen geographical region. We use this population count as an empirical probability distribution  $\text{Pr}(\phi, \lambda|\Psi)$ , where  $\Psi$  is population count and  $\phi, \lambda$  are the geographic coordinates of a grid cell. Thereby, highly traveled roads and routes, where population is high, are favored over routes in remote and less populated regions. The procedure is described in Algorithm 3. In the algorithm, we utilize the Haversine formula to calculate the air-line distance  $d_{air}$ , or "as-the-crow-flies" distance, between the start point and a potential destination as a first estimate of the route length [47].

Using the TRDB, the fastest route  $\pi$  is calculated from the start point to the destination based on the speed profile  $u$  derived from mean traffic speed. Using the geographic coordinates of the route  $(\phi_k, \lambda_k)$ , nearby CPs can be found. In this work, we use an open database to collect information such as CP location and charging power of the current day charging infrastructure [41]. The CPs and the start and destination constitute the vertices of the trip's directed graph  $\mathcal{G}$ . The weights of the edges between the vertices represent the travel time for each edge, which again is determined using the

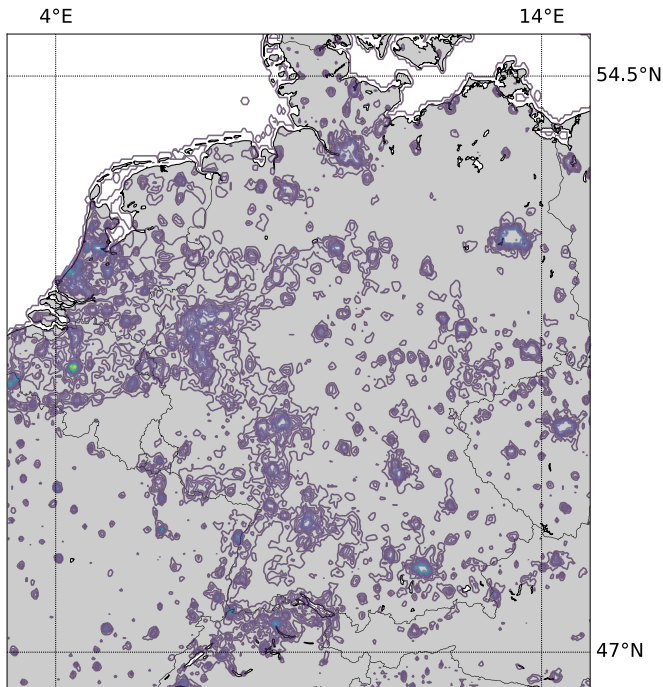


FIGURE 8. Contour plot of the population data used as a probability distribution for start and destination points.

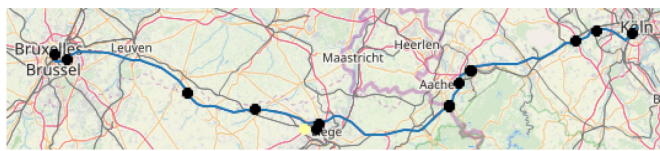


FIGURE 9. Example route with charging points. Map data (c) OpenStreetMap contributors.

---

**Algorithm 3:** Draw Samples: Start and Destination.

---

draw sample  $d_{\text{desired}}$  from  $\text{Pr}(d)$   
draw sample  $(\phi_1, \lambda_1)$  from  $\text{Pr}(\Psi|\phi, \lambda)$   
initialize air-line distance  $d_{\text{air}} \neq d_{\text{desired}}$   
**while**  $d_{\text{air}} \neq d_{\text{desired}}$  **do**  
    draw sample  $(\phi_2, \lambda_2)$  from  $\text{Pr}(\Psi|\phi, \lambda)$   
    estimate air-line distance  
     $d_{\text{air}} = R \cdot \text{archav}(\phi_2, \lambda_2, \phi_1, \lambda_1)$   
**Result:**  $(\phi_1, \lambda_1)$  and  $(\phi_2, \lambda_2)$

---

TRDB. Additionally, for each directed edge, the road segment information is extracted from the TRDB. This information is necessary for the powertrain simulation model. The route sampling is independent from the chosen vehicle, as the routes  $\pi$  and speed profiles  $u$  do not exceed the limitations of our vehicle models. An exemplary route with CPs can be seen in Fig. 9.

**C. ENERGY CONSUMPTION ESTIMATION AND CHARGING PLAN**

For each trip and vehicle-battery combination, the energy consumption is simulated with the model introduced in Section II-C. The velocity acquired from the TRDB is assumed to be the exact speed of the vehicle. As information about acceleration is missing, we use the change in kinetic energy between road segments to compensate for the missing acceleration data. The energy consumed on segment  $k$  is:

$$E_{c,k} = \underbrace{\int \frac{F_{r,k}}{\eta_{\text{stat}}(F_{r,k}, u_k)} ds}_{\tilde{E}_{c|a=0}} + \underbrace{\frac{m}{2\eta_{\text{dyn}}} [(u_{k+1})^2 - (u_k)^2]}_{\Delta E_{\text{kin}}} + \frac{l_k P_{\text{aux},k}}{u_k}, \quad (10)$$

which directly follows from (4) when using traffic speed  $u$ . The last term encompasses the additional energy consumed by auxiliary equipment, such as infotainment and HVAC systems, which together draw power  $P_{\text{aux}}$ . The total energy needed for a trip is thus

$$E_c = \sum_{i \in \pi} \sum_{k \in i} E_{c,k} = \sum_{i \in \pi} E_{c,i}, \quad (11)$$

where  $\pi$  is the given route, consisting of edges  $i$ , which consist of segments  $k$ .

$P_{\text{aux}}$  is constant in all simulations and is based on mean temperature in our chosen geographical region. The total power drawn by auxiliary equipment is estimated to be 1.5kW. In very hot or very cold weather conditions, the power demand of the auxiliaries can be significantly higher, however we do not consider these corner cases in our model.

At the beginning of each simulation, an energy consumption prediction is calculated. Instead of calculating this prediction explicitly as done in Section III-B, an implicit prediction is done. Using the energies required for the graph's edges  $E_{c,i}$  and the known error distribution from Section III-D, we implicitly calculate an EDP for each edge  $i$  of the graph, i.e. for each leg of the route:

$$E_{c,i} = \tilde{E}_{c,i} + e \cdot l_i, \quad (12)$$

where  $l_i$  is the edge length and  $e$  is the error in the EDP drawn from the known error distribution. Alternatively,  $e$  can be drawn from other distributions, such as

$$e \sim \mathcal{N}(\mu, \sigma^2), \quad (13)$$

to simulate the error distributions of other algorithms. In this way, the impact of better or worse performing range estimation algorithms can be examined. The predicted total energy consumed on the route is thus:

$$\tilde{E}_c = \sum_{i \in \pi} \tilde{E}_{c,i}. \quad (14)$$

As discussed in Section III, an EDP is always subject to uncertainty. Therefore, a certain part of available battery energy needs to be reserved at CPs and other destinations. This safety

---

**Algorithm 4:** Charging Planner.

using  $\tilde{E}_{c,k}$ ,  $P(\mathcal{V})$ , vehicle, start SoC, ...  
**for** each vertex  $\mathcal{V}$  with CP  $P_{\mathcal{V}}$  **do**  
     | calculate necessary charging energy  $\Delta E_b(\mathcal{V}, E_c)$   
     | calculate charging time  $\tau(\Delta E_b)$   
 pre-process  $\mathcal{G}' = \mathcal{G} + \tau$   
 calculate fastest path  $\pi'$  with Dijkstra's algorithm.  
**Result:**  $\pi'$  - fastest route with necessary charging stops

---

margin  $\Delta b_E$  is based on the error distribution of the EDP. The maximum length of traversable edges is limited by the specific maximum range  $R_{max}$  of the vehicle:

$$R_{max} = (1 - \Delta b_E) \frac{Q}{dE_c/ds}. \quad (15)$$

To determine a suitable  $\Delta b_E$ , the following condition must be satisfied:

$$e_{max} R_{max} \leq \Delta b_E Q, \quad (16)$$

with  $e_{max}$  being the maximum probable error in terms of energy per distance. This leads to

$$\Delta b_E \geq \left( \frac{dE_c/ds}{e_{max}} + 1 \right)^{-1}. \quad (17)$$

If the sum of  $\tilde{E}_c$  and  $\Delta b_E \hat{E}_b$  is larger than the available battery energy corresponding to the current SoC,  $\hat{E}_b$ , charging stops need to be planned.

Charge planning has been studied extensively to enable time- or energy-optimal routing for electric vehicles [48]–[51]. To prepare the planning of charging stops, the amount of electrical energy needed to charge at each possible charging stop is determined and the corresponding charging time  $\tau$  is then calculated using the relation

$$\tau = \int_{\hat{E}_{b,start}}^{\hat{E}_{b,end}} \frac{dE}{\min(P(E), P_{\mathcal{V}})}. \quad (18)$$

Here,  $\hat{E}_{b,start}$  and  $\hat{E}_{b,end}$  are the battery states of energy (SoEs) at beginning and end of charging, respectively,  $P_{\mathcal{V}}$  is the available CP power at vertex  $\mathcal{V}$  and  $P(E)$  is the possible charging power at SoE  $\hat{E}_b = qQ$ . The charging times  $\tau$  are then used to pre-process the travel time graph  $\mathcal{G}$  and the fastest path from start to destination can be calculated with Dijkstra's algorithm [52]. The procedure is shown in Algorithm 4.

#### D. TRIP SIMULATION

Ultimately, the trip simulation is carried out as shown in Algorithm 5. Results obtained by varying the parameters are analyzed in Section V.

#### V. SIMULATION RESULTS

In this section, the simulation runs are executed with the parameter variation presented in Section IV. The investigation aims at examining effects of range estimation accuracy,

---

**Algorithm 5:** Trip Simulation.

calculate fastest route  $\pi$   
 calculate EDP:  $\tilde{E}_c$  with (14)  
**if**  $\tilde{E}_c > (1 - \Delta b_E) \hat{E}_b$  **then**  
     | plan charging stops with Algorithm 4  
 start driving at vertex  $\mathcal{V} = 0$   
**for** each edge  $i = 1, 2, \dots$  in route  $\pi$  **do**  
     **for** each segment  $k = 1, 2, \dots$  in edge  $i$  **do**  
         | simulate  $E_{c,k}^{driven}$  with (10)  
          $E_{c,i} = \sum_{k \in i} E_{c,k}$   
          $\hat{E}_b -= E_{c,i}$   
         re-calculate  $\tilde{E}_{c,i}$  for remaining edges  $i$   
         **if**  $\hat{E}_b < 0$  **then**  
             | vehicle stranded  
         **else if**  $\tilde{E}_{c,i+1} > (1 - \Delta b_E) \hat{E}_b$  **then**  
             | plan additional charging stops with Algorithm 4  
         **else if**  $\mathcal{V}$  is planned charging stop **then**  
             | charge battery  
         **else**  
             | continue

---

vehicle concepts and charging infrastructure. We use the performance indicator travel time to represent the results, as well as the proportion of travel time spent charging. The travel time comprises driving time, charging time and time overhead for authentication and handling at the CP. Since the total travel time is the sum of driving time and charging time, travel time and charging time can be visualized in one diagram where total driving time is a constant. The driving time is calculated using the speed profile  $u$  derived from mean traffic speed. The charging time is calculated with (18), where the characteristic charging curves are modeled from real data. Based on our measurements, the time overhead at a CP is 2.5min on average. Since the terms in the calculation of total travel time are independently valid, we assume that the travel time is valid as well. Furthermore, numerous conclusions can be drawn from the characteristics of the results irrespective of their absolute numerical values.

#### A. RANGE ESTIMATION ACCURACY

To analyze the effect of EDP accuracy, we consider a mid-size vehicle, as the error distribution was determined using real data from this class of vehicles. The mid-size vehicle is simulated with the six different EDP algorithm variants and the necessary safety margin  $\Delta b_E$ , while other settings remain constant. The corresponding safety margin values calculated with (17) are shown in Table 5. There, we use the subscript  $a$  to denote the error distribution of the anonymous dataset and  $d$  for the driver-specific dataset. In addition, we introduce two synthetic algorithms ST<sub>10%</sub> and ST<sub>5%</sub>.

It can be seen that the algorithms using driver-specific information lead to lower safety margins, between 13% and

TABLE 5. Safety Margins

Algorithm	$\Delta b_E$
$u_d$	16 %
MLR <sub>d</sub>	13 %
SVM <sub>d</sub>	16 %
$u_a$	19 %
MLR <sub>a</sub>	20 %
SVM <sub>a</sub>	25 %

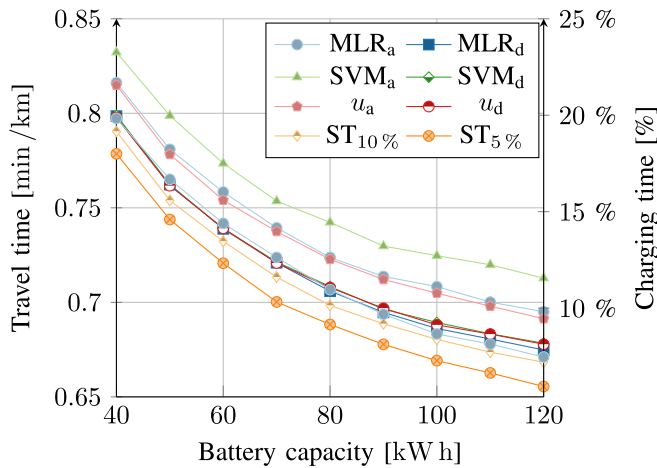


FIGURE 10. Travel time (left axis) and charging time as a percentage of driving time (right axis) for different EDP algorithms for a mid-size vehicle with different battery capacities in current charging infrastructure.

16%. Consequently, the standard algorithm using only traffic data  $u_d$  leads to the same safety margin as the most complex algorithm SVM<sub>d</sub>. Using MLR, the safety margin can be 3% lower. Using an algorithm which does not save driver-specific information between trips leads to safety margins between 19% and 25%. Here, the standard algorithm using only traffic data  $u_a$  achieves the lowest safety margin.

Before the simulated test runs start, the SoC at the beginning of each trip is set to 40%, thus a higher percentage of routes include at least one charging stop. This means that the resulting travel times could be somewhat longer than in the best case, when each trip starts with a fully charged battery. Nonetheless, a direct comparison between algorithms is presented.

The resulting travel and charging times for different range estimation accuracy for a mid-sized vehicle are shown in Fig. 10. The diagram shows the values with respect to total travel time divided by total distance driven and with respect to the amount of charging time divided by travel time. Travel and charging times decrease with a decreasing safety margin. Apparently, the 3% advantage in safety margin between MLR<sub>d</sub> and  $u_d$  does not lead to a significant decrease in travel time. Here, we point out that comparisons between anonymous and data-specific algorithms cannot be made correctly, since the dataset is different.

However, to show the significance of accurate range estimation algorithms, we included two synthetic results ST with 5% and 10% safety margin. It can be seen that a vehicle using

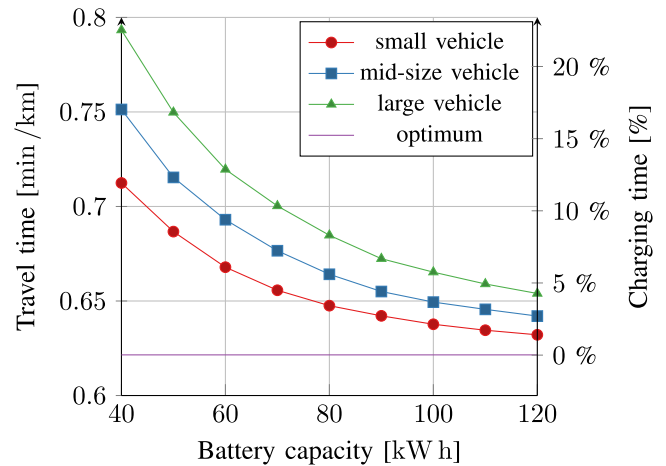


FIGURE 11. Travel time (left axis) and charging time as a percentage of travel time (right axis) for different vehicle concepts and battery capacities in current charging infrastructure.

ST<sub>5%</sub> achieves the same travel time with 90kWh as a vehicle with MLR<sub>d</sub> and 120kWh. Thus, an 8% difference in safety margin translates to a virtual battery capacity difference of 30kWh. It shows that high range estimation accuracy could provide automobile manufacturers with a significant potential for smaller batteries which saves weight, money and space. Still, ST<sub>5%</sub> is a synthetic result and therefore, in the following sections, we will use MLR<sub>d</sub> to analyze the influence of further features and parameters.

## B. VEHICLE CONCEPTS

In this section, we analyze the behavior of the three different vehicle concepts presented in Table 4. From this simulation, we can analyze the interaction of battery capacity, efficiency and travel time in the current road and charging infrastructure.

The results for total travel time divided by total distance driven are shown in Fig. 11, as well as total time spent charging as a percentage of travel time. The total travel time decreases with increasing battery capacities, as well as for a vehicle concept with a higher efficiency. The rate of change in travel time is quite high at smaller battery capacities but with increasing capacity it reaches a certain saturation. Here, most of the trips can be finished with short charging stops or without any stops whatsoever. This suggests that batteries do not need to exceed 100kWh. A vehicle with unlimited battery capacity, i.e. without the necessity of charging stops, would take 0.62min/km to drive all routes sampled. That value is denoted *optimum* in Fig. 11.

Smaller and more efficient vehicles also need smaller batteries to achieve the same travel time. For example, let us specify that travel time should be less than 0.66min/km. Then, the necessary battery capacity can be calculated for each of the vehicle concepts. To achieve this travel time, the large vehicle needs a 120kWh battery, the mid-size vehicle 90kWh and the small vehicle a 70kWh battery. However, the travel

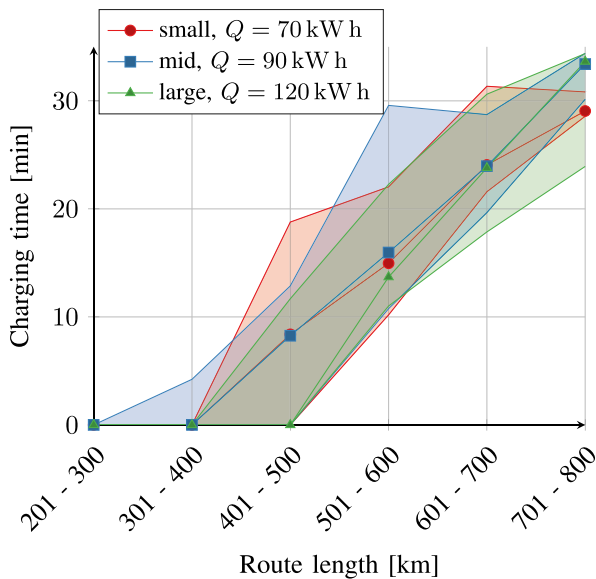


**FIGURE 12.** Charging time for different vehicle concepts and route length clusters in current charging infrastructure.

and charging time also depends on selected trip length. Therefore, we cluster all the simulated trips with respect to their length and compare charging times, as shown in Fig. 12. The connected dots represent the median charging time in minutes and the shaded areas demarcate the interval between the 5th and 95th percentiles. Although all vehicle concepts have approximately the same total travel time, there are significant differences in charging time when looking only at trips of a certain length. An important factor in the overall usability of BEVs is the long-distance capability, i.e. the capability of covering the distance between charging points (CPs) on a route. In sparse charging infrastructures, large battery capacity and/or low energy consumption resulting in high total driving range is necessary. In dense infrastructures, the total range is only of secondary importance.

### C. CHARGING POINT POWER

The current charging infrastructure is highly variable between regions and is constantly growing, both in terms of CP numbers and power. To analyze the effects of CP power on travel time, a simulation is executed where the power of current CPs is varied. In the first variation, all CPs can output only a maximum of 50kW, in the second variation a maximum of 150kW, the third variation is the current charging infrastructure and in the fourth variation, all CPs can output 350kW. The total number of CPs is held constant between the variations.

Fig. 13 shows total travel and charging time for a mid-sized vehicle with different battery capacities in the four infrastructure variations. We observe that the current charging infrastructure is clearly much better than if all CPs were limited to 50kW, especially with larger battery capacities that are not limited by the maximal  $C$ -Rate of  $3h^{-1}$ . The improvement

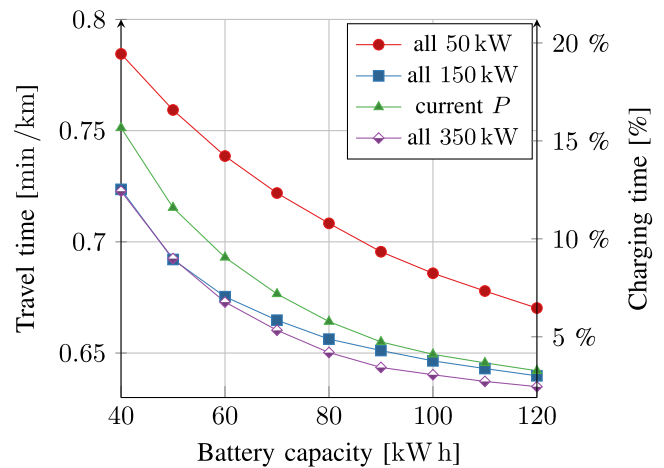


**FIGURE 13.** Travel time (left axis) and charging time as a percentage of travel time (right axis) for a mid-size vehicle with different battery capacities in four charging power variations.

of increasing charging power of all CPs to 350kW also reduces travel and charging time significantly. This reduction can especially be observed with smaller battery capacities, since charging stop frequency is higher and a dense network of CPs is required. Similarly, the time reduction for vehicles with larger battery capacities is smaller partially because of the lower frequency of charging stops. In the variation where all CPs have a maximum charging power of 150kW, the travel time improvement for smaller battery capacities is the same or close to the improvement of the 350kW variation, as their maximal  $C$ -Rate corresponds to maximum charging power  $\ll 350kW$ . On the other hand, travel time in vehicles with larger battery capacities is only slightly better than in the current infrastructure.

### D. CHARGING POINT DENSITY

In addition to CP power, CP density is variable and will increase in the future. In order to analyze the effect of CP density, we modify the data of the current, real charging infrastructure in the chosen geographical region, by either reducing or increasing the density of CPs along a route. Let the density of current charging infrastructure be  $D = 1$ . In addition,  $D = 1^+$  denotes current density where all CPs can output 350kW. We reduce the density by randomly removing a portion of the CPs in the database, resulting in densities such as  $D = 0.75$  and  $D = 0.5$ . Additionally,  $D = 0.75^+$  denotes a variation where all CPs can output 350kW. Creating new CPs would be tedious and difficult and instead we analyze the edge case of a perfect infrastructure, where every point on the route is a 350kW CP, resulting in a density of  $D \rightarrow \infty^+$ .

Fig. 14 shows total travel and charging time for a mid-sized vehicle with different battery capacities in six infrastructure variations. It can be seen that a higher density of CPs leads to shorter travel and charging times for all battery capacities. The variation  $D = 0.75^+$  shows an improvement in travel time as well. The slope of the curves corresponds to the rate of change

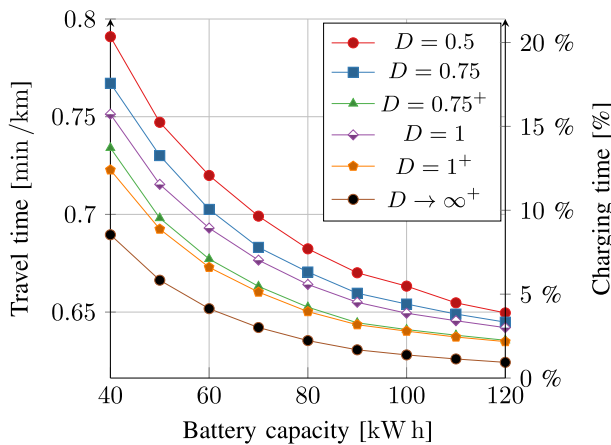


**FIGURE 14.** Travel time (left axis) and charging time as a percentage of travel time (right axis) for a mid-size vehicle with different battery capacities in six CP density variations.

in travel time with increasing battery capacity. In sparse charging infrastructures, travel and charging times continue to decrease with increasing battery capacities beyond 100 kWh. In more dense charging infrastructures, a saturation in travel and charging time can be observed. Furthermore, robustness against sparse infrastructure increases with increasing battery capacity, i.e. a larger battery is less sensitive to sparse charging infrastructures and travel and charging times are proportionally closer to the times in a perfect infrastructure.

## VI. CONCLUSION AND OUTLOOK

In this work, we investigated the everyday usability of electric vehicles. We chose the amount of time consumed per trip as a mathematical equivalent to the everyday usability, as this encompasses the ultimate goal of mobility: bringing people from A to B as quickly as possible. The difference between electric vehicles compared to conventional ones, lies in the limited driving range and charging time and infrastructure. Therefore, we concentrated on these aspects when executing a stochastic trip simulation. We drew random trips with different vehicle parameters as well as charging points to display the influence of relevant features.

One central outcome was the feasibility limit of battery capacity. One would think increasing battery capacity endlessly would solve the challenges of electric mobility and of course, bigger batteries mean less trip duration. However, there is a feasibility limit around 100kWh. Beyond this, increasing battery capacity does not improve travel time significantly. At this point, the impact of an improved charging point network on the everyday usability is stronger. In our results, charging times of around 5 - 20% are common in the current charging infrastructure. This can be decreased to below 5% in a perfect infrastructure.

In addition, smaller vehicles have less energy consumption and that translates to less travel time. Of course, smaller vehicles typically also have smaller batteries which increases their travel time again. However, a smaller vehicle can achieve the

same travel time as a large vehicle with less battery capacity. Therefore, their battery *can* be smaller since energy efficiency is higher. Lastly, having more accurate range estimation algorithms means less travel time and effectively increases the usable battery capacity, as the safety margin is smaller. This could be a more cost efficient choice than increasing total battery capacity. Other drawbacks of larger batteries are packaging, weight, and environmental effects, all of which do not hold for range estimation software. However, the algorithms tests in our framework did not achieve significant advantages. Only the synthetic results could show the potential of lower safety margins.

Finding more accurate range estimation algorithms and quantifying the advantage in terms on trip duration is one aspect for further research. Another aspect would be the integration of aging effects in battery as well as powertrain. The availability of charging at home or at a workplace is an interesting aspect that could be analyzed and integrated in the framework. Including environmental effects such as wind, precipitation etc. in the framework would enable the analysis of more detailed scenarios. Additionally, more data from other countries could be used for the stochastic model in the future.

Apart from that, the central outcome of this research can be summarized as: *Battery sizes of modern premium BEVs are already large enough.* We do not need to increase them much further, however we have a long way ahead of us in terms of charging infrastructure.

## REFERENCES

- [1] J. Dong, X. Wu, C. Liu, Z. Lin, and L. Hu, "The impact of reliable range estimation on battery electric vehicle feasibility," *Int. J. Sustain. Transp.*, vol. 14, no. 11, pp. 833–842, Nov. 2019. [Online]. Available: <https://doi.org/10.1080/15568318.2019.1639085>
- [2] M. A. Melliger, O. P. van Vliet, and H. Liimatainen, "Anxiety vs reality – sufficiency of battery electric vehicle range in switzerland and finland," *Transp. Res. Part D: Transport Environ.*, vol. 65, pp. 101–115, Dec. 2018.
- [3] G. Pasaoglu, A. Zubaryeva, D. Fiorello, and C. Thiel, "Analysis of European mobility surveys and their potential to support studies on the impact of electric vehicles on energy and infrastructure needs in Europe," *Technol. Forecasting Social Change*, vol. 87, pp. 41–50, Sep. 2014.
- [4] C. J. Meinrenken, Z. Shou, and X. Di, "Using GPS-data to determine optimum electric vehicle ranges: A Michigan case study," *Transp. Res. Part D: Transport Environ.*, vol. 78, Jan. 2020, Art. no. 102203.
- [5] A. Zhang, J. E. Kang, and C. Kwon, "Multi-day scenario analysis for battery electric vehicle feasibility assessment and charging infrastructure planning," *Transp. Res. Part C: Emerg. Technol.*, vol. 111, pp. 439–457, Feb. 2020.
- [6] J. Dong and Z. Lin, "Stochastic modeling of battery electric vehicle driver behavior," *Transp. Res. Rec.: J. Transp. Res. Board*, vol. 2454, no. 1, pp. 61–67, Jan. 2014.
- [7] A. Meintz *et al.*, "Enabling fast charging – vehicle considerations," *J. Power Sources*, vol. 367, pp. 216–227, Nov. 2017.
- [8] R. Smith, S. Shahidinejad, D. Blair, and E. Bibeau, "Characterization of urban commuter driving profiles to optimize battery size in light-duty plug-in electric vehicles," *Transp. Res. Part D: Transport Environ.*, vol. 16, no. 3, pp. 218–224, May 2011.
- [9] Z. Lin, "Optimizing and diversifying electric vehicle driving range for U.S. drivers," *Transp. Sci.*, vol. 48, no. 4, pp. 635–650, Nov. 2014.
- [10] M. D. Gennaro, E. Paffumi, G. Martini, and H. Scholz, "A pilot study to address the travel behaviour and the usability of electric vehicles in two Italian provinces," *Case Stud. Transport Policy*, vol. 2, no. 3, pp. 116–141, Dec. 2014.

- [11] Z. A. Needell, J. McNerney, M. T. Chang, and J. E. Trancik, "Potential for widespread electrification of personal vehicle travel in the United States," *Nature Energy*, vol. 1, no. 9, pp. 16112–16118, Aug. 2016. [Online]. Available: <https://doi.org/10.1038/nenergy.2016.112>
- [12] N. S. Pearre, W. Kempton, R. L. Guensler, and V. V. Elango, "Electric vehicles: How much range is required for a day's driving?" *Transp. Res. Part C: Emerg. Technol.*, vol. 19, no. 6, pp. 1171–1184, Dec. 2011.
- [13] X. Shi, J. Pan, H. Wang, and H. Cai, "Battery electric vehicles: What is the minimum range required?" *Energy*, vol. 166, pp. 352–358, Jan. 2019.
- [14] Z. Li, S. Jiang, J. Dong, S. Wang, Z. Ming, and L. Li, "Battery capacity design for electric vehicles considering the diversity of daily vehicles miles traveled," *Transp. Res. Part C: Emerg. Technol.*, vol. 72, pp. 272–282, Nov. 2016.
- [15] Z. Yi and P. H. Bauer, "Optimization models for placement of an energy-aware electric vehicle charging infrastructure," *Transp. Res. Part E: Logistics Transp. Rev.*, vol. 91, pp. 227–244, Jul. 2016.
- [16] F. Xie, C. Liu, S. Li, Z. Lin, and Y. Huang, "Long-term strategic planning of inter-city fast charging infrastructure for battery electric vehicles," *Transp. Res. Part E: Logistics Transp. Rev.*, vol. 109, pp. 261–276, Jan. 2018.
- [17] P. Jochem, C. Brendel, M. Reuter-Oppermann, W. Fichtner, and S. Nickel, "Optimizing the allocation of fast charging infrastructure along the German Autobahn," *J. Bus. Econ.*, vol. 86, no. 5, pp. 513–535, Oct. 2015.
- [18] A. Ashtari, E. Bibeau, S. Shahidinejad, and T. Molinski, "PEV charging profile prediction and analysis based on vehicle usage data," *IEEE Trans. Smart Grid*, vol. 3, no. 1, pp. 341–350, Mar. 2012.
- [19] J. R. Helmus, S. Wachlin, I. Vermeulen, and M. H. Lees, "SEVA: A data driven model of electric vehicle charging behavior," 2019, *arXiv:1904.08748*.
- [20] M. B. Arias, M. Kim, and S. Bae, "Prediction of electric vehicle charging-power demand in realistic urban traffic networks," *Appl. Energy*, vol. 195, pp. 738–753, Jun. 2017.
- [21] P. Olivella-Rosell, R. Villafafila-Robles, A. Sumper, and J. Bergas-Jané, "Probabilistic agent-based model of electric vehicle charging demand to analyse the impact on distribution networks," *Energies*, vol. 8, no. 5, pp. 4160–4187, May 2015.
- [22] T. S. Bryden, G. Hilton, A. Cruden, and T. Holton, "Electric vehicle fast charging station usage and power requirements," *Energy*, vol. 152, pp. 322–332, Jun. 2018.
- [23] T. Gnann, S. Funke, N. Jakobsson, P. Plötz, F. Sprei, and A. Bennehag, "Fast charging infrastructure for electric vehicles: Today's situation and future needs," *Transp. Res. Part D: Transport Environ.*, vol. 62, pp. 314–329, Jul. 2018.
- [24] J. Neubauer and E. Wood, "The impact of range anxiety and home, workplace, and public charging infrastructure on simulated battery electric vehicle lifetime utility," *J. Power Sources*, vol. 257, pp. 12–20, Jul. 2014.
- [25] S. Sautermeister, F. Ott, M. Vaillant, and F. Gauterin, "Reducing Range Estimation Uncertainty with a Hybrid Powertrain Model and Online Parameter Estimation," *Proc. IEEE Int. Conf. Intell. Transp. Syst. (ITSC)*, 2017, pp. 1–6.
- [26] S. Sautermeister, M. Falk, B. Bäker, F. Gauterin, and M. Vaillant, "Influence of Measurement and Prediction Uncertainties on Range Estimation for Electric Vehicles," *IEEE Trans. Intell. Transp. Syst.*, vol. 19, no. 8, pp. 2615–2626, Aug. 2018.
- [27] S. Scheubner, A. Thorgeirsson, M. Vaillant, and F. Gauterin, "A Stochastic Range Estimation Algorithm for Electric Vehicles Using Traffic Phase Classification," *IEEE Trans. Veh. Technol.*, vol. 68, no. 7, pp. 6414–6428, Jul. 2019.
- [28] R. Jazar, *Vehicle Dynamics: Theory and Application*. Berlin, Germany: Springer, 2014.
- [29] T. Franke, I. Neumann, F. Bühler, P. Cocron, and J. Krems, "Experiencing Range in an Electric Vehicle - Understanding Psychol. Barriers," *Appl. Psychol.: Int. Rev.*, vol. 61, no. 3, pp. 368–391, 2012.
- [30] HERE Global B.V., "Routing API Developer's Guide," 2020. [Online]. Available: [http://developer.here.com/...documentation/routing/dev\\_guide/topics/%20resources.html](http://developer.here.com/...documentation/routing/dev_guide/topics/%20resources.html)
- [31] Y. Su, X. Gao, X. Li, and D. Tao, "Multivariate Multilinear Regression," *IEEE Trans. Syst., Man, Cybern. - Part B: Cybern.*, vol. 42, no. 6, pp. 1560–1573, Dec. 2012.
- [32] W. Ambrosius, *Topics in Biostatistics*. ser. Methods in Molecular Biology Series. Totowa, NJ, USA: Humana Press Inc., 2008, vol. 404.
- [33] P. J. Huber and E. M. Ronchetti, *Robust Statistics*. ser. Wiley Series in Probability and Mathematical Statistics. Hoboken, NJ, USA: Wiley, 1981.
- [34] C. Wu, J. Ho, and D. Lee, "Travel-time prediction with support vector regression," *IEEE Trans. Intell. Transp. Syst.*, vol. 5, no. 4, pp. 276–281, Dec. 2004.
- [35] L. Vanajakshi and L. Rilett, "A comparison of the performance of artificial neural networks and support vector machines for the prediction of traffic speed," in *Proc. IEEE Intell. Vehicles Symp.*, 2004, pp. 194–199.
- [36] A. Smola and B. Schölkopf, "A tutorial on support vector regression," *Statist. Comput.*, vol. 14, pp. 199–222, 2004.
- [37] A. Tomaszewska et al., "Lithium-ion battery fast charging: A review," *eTransportation*, vol. 1, Aug. 2019, Art. no. 100011.
- [38] Tesla Inc., "Introducing V3 Supercharging," Mar. 2019. [Online]. Available: <https://www.tesla.com/blog/introducing-v3-supercharging>
- [39] B. Lincoln, "Tesla battery charging data from 801 cars," Nov. 2018. [Online]. Available: <https://forum.abetterrouteplanner.com/blogs/entry/6-tesla-battery-charge-ing-data-from-801-cars/>
- [40] J. Voelcker, "Porsche's fast-charge power play: The new, all-electric Taycan will come with a mighty thirst. this charging technology will slake it," *IEEE Spectr.*, vol. 56, no. 09, pp. 30–37, Sep. 2019.
- [41] "Goingelectric stromtankstellen statistik," 2020. [Online]. Available: <https://www.goingelectric.de/stromtankstellen/statistik/Deutschland/>
- [42] G.-L. Zhu et al., "Fast charging lithium batteries: Recent progress and future prospects," *Small*, vol. 15, no. 15, Mar. 2019, Art. no. 1805389.
- [43] P. Plötz, N. Jakobsson, and F. Sprei, "On the distribution of individual daily driving distances," *Transp. Res. Part B: Methodol.*, vol. 101, pp. 213–227, Jul. 2017.
- [44] Federal Highway Administration, *2017 National Household Travel Survey*. U.S. Dept. Transportation, Washington, DC, USA, 2017. [Online]. Available: <https://nhts.ornl.gov>
- [45] G. Pasaoglu et al., "Driving and parking patterns of European car drivers - A mobility survey," Eur. Commission Joint Res. Centre, Luxembourg, Belgium, 2012.
- [46] Center For International Earth Science Information Network-CIESIN-Columbia University, "Gridded population of the world, version 4 (GPWv4): Population count adjusted to match 2015 revision of UN WPP country totals, revision 11," 2018. [Online]. Available: <http://sedac.ciesin.columbia.edu/data/set/gpw-v4-population-count-adjusted-to-2015-unwpp-country-totals-rev11>
- [47] M. J. De Smith, M. F. Goodchild, and P. Longley, *Geospatial Analysis: A Comprehensive Guide to Principles, Techniques and Software Tools*. Kibworth Harcourt, U.K.: Troubador publishing ltd, 2007.
- [48] M. Baum, J. Dibbelt, A. Gemsa, D. Wagner, and T. Zündorf, "Shortest feasible paths with charging stops for battery electric vehicles," *Transp. Sci.*, vol. 53, no. 6, pp. 1627–1655, Nov. 2019.
- [49] S. Schoenberg and F. Dressler, "Planning ahead for EV: Total travel time optimization for electric vehicles," in *Proc. IEEE Intell. Transp. Syst. Conf.*, Oct. 2019, pp. 3068–3075. [Online]. Available: <https://doi.org/10.1109/itsc.2019.8917335>
- [50] M. Schiffer and G. Walther, "The electric location routing problem with time windows and partial recharging," *Eur. J. Oper. Res.*, vol. 260, no. 3, pp. 995–1013, Aug. 2017.
- [51] M. Alizadeh, H.-T. Wai, A. Scaglione, A. Goldsmith, Y. Y. Fan, and T. Javidi, "Optimized path planning for electric vehicle routing and charging," in *Proc. 52nd Annu. Allerton Conf. Commun., Control, Comput. (Allerton)*, Sep. 2014, pp. 25–32.
- [52] E. W. Dijkstra, "A note on two problems in connexion with graphs," *Numer. Math.*, vol. 1, no. 1, pp. 269–271, 1959.



**ADAM THOR THORGEIRSSON** received the B.Sc. degree in mechanical engineering from the University of Iceland, Reykjavik, Iceland, in 2014, and the M.Sc. degree in mechanical engineering from the Karlsruhe Institute of Technology (KIT), Karlsruhe, Germany, in 2017. He is currently working toward the doctoral degree with Dr. Ing. h.c. F. Porsche AG and supervised by Frank Gauterin (KIT).



**STEFAN SCHEUBNER** received the B.Sc. and M.Sc. degrees in mechanical engineering from the Karlsruhe Institute of Technology (KIT), Karlsruhe, Germany, in 2011 and 2015, respectively, and the M.Sc. degree in mechanical engineering from the Korean Advanced Institute of Science and Technology (KAIST), Daejeon, South Korea, in 2015. From 2015 to 2020, he worked on energy management functions for BEVs with Porsche AG. Since then, he is concerned with dc fast-charging infrastructure for BEVs with EnBW AG.



**SEBASTIAN FÜNFELD** received the M.Sc. degree in mechanical engineering from Karlsruhe Institute of Technology (KIT), Karlsruhe, Germany, in 2014. From 2014, he has been with Dr. Ing. h.c. F. Porsche AG, Weissach, Germany. His research interests focus on intelligent control and predictive systems, including modeling of driver and traffic behavior, stochastic forecasting, and stochastic optimization



**FRANK GAUTERIN** received the diploma degree in physics from the University of Munster, Munster, Germany, in 1989 and the Dr. rer. nat. degree (Ph.D.) in physics from the University of Oldenburg, Oldenburg, Germany, in 1994. From 1989 to 2006, he was in different R&D positions with Continental AG, Germany, leaving as the Director of NVH Engineering (noise, vibration, harshness). Since 2006, he has been a Full Professor with the Karlsruhe Institute of Technology (KIT), Karlsruhe, Germany. He is the Head of the KIT Institute of Vehicle System Technology and scientific spokesperson of the KIT Center Mobility Systems. His research interests include vehicle control, vehicle dynamics, vehicle NVH, vehicle suspension, tire dynamics and tire-road-interaction as well as vehicle concepts, vehicle modeling, and identification methods.